Large Eddy Simulation and RANS Analysis of the End-Wall Flow in a Linear Low-Pressure-Turbine Cascade: Part II - Loss Generation

LES and RANS Analysis of the End-Wall Flow in a Linear LPT Cascade: Part II – Loss Generation

Michele Marconcini*
Roberto Pacciani
Andrea Arnone
Dept. of Industrial Engineering
University of Florence
via di Santa Marta, 3, 50139 Florence, Italy
michele.marconcini@unifi.it

Vittorio Michelassi
Baker Hughes, a GE Company
Via Felice Matteucci 10,
50127, Florence, Italy
vittorio.michelassi@bhge.com

Richard Pichler
Yaomin Zhao
Richard Sandberg
Dept. of Mechanical Engineering
University of Melbourne
Parkville, Victoria 3010, Australia
richard.sandberg@unimelb.edu.au

ABSTRACT

In low-pressure-turbines (LPT) at design point around 60-70% of losses are generated in the blade boundary layers far from end-walls, while the remaining 30%-40% is controlled by the interaction of the blade profile with the end-wall boundary layer. Increasing attention is devoted to these flow regions in industrial design processes. This paper discusses the end-wall flow characteristics of the T106 profile with parallel end-walls at realistic LPT conditions, as described in the experimental setup of Duden and Fottner (1997) P. I. Mech. Eng. A-J. Pow., 211 (4), pp.309-320. Calculations

*Corresponding author

are carried out by both RANS, due to its continuing role as the design verification workhorse, and highly-resolved LES. Part II of the paper focuses on the loss generation associated with the secondary end-wall vortices. Entropy generation and the consequent stagnation pressure losses are analyzed following the aerodynamic investigation carried out in the companion paper (GT2018-76233). The ability of classical turbulence models generally used in RANS to discern the loss contributions of the different vortical structures is discussed in detail and the attainable degree of accuracy is scrutinized with the help of LES and the available test data. The purpose is to identify the flow features that require further modelling efforts in order to improve RANS/URANS approaches and make them able to support the design of the next generation of LPTs.

INTRODUCTION

In low-pressure-turbines, profile losses cover around 60-70% of the inefficiency, while the remaining 30-40% are generated close to end-walls by the growth of secondary vorticity. At off-design conditions, end-wall losses may grow higher than the percentage indicated above, especially for highly-loaded LPT designs often sought after by engine designers to reduce weight and cost. Although cavities and purge flows affect the secondary flow pattern details (Popović and Hodson [1]), still a lot can be understood by looking at the secondary vortex growth in a turbine vane or blade end-wall region with smooth walls.

Experimental research did shed light on the mechanism that controls the growth of the secondary vortices. The works of Hodson and Dominy [2, 3], Gregory-Smith et al. [4], Walsh and Gregory Smith [5], Gregory-Smith and Cleak [6], and Infantino et al. [7], are only some examples of experimental studies on the secondary flow evolution in turbine cascades at design and off-design conditions. The review papers by Sieverding [8] and Langston [9] provide an extensive summary of the results of several decades of investigations on linear cascades.

Low-pressure-turbine (LPT) profiles losses have been successfully analyzed with the aid of LES and DNS [10] as well as URANS [11, 12]. Koschichow et al. [13] used DNS to study the secondary flow dynamics, the associated losses in the attempt to shed more light on this complex flow region. The work by Cui et al. [14] has demonstrated how LES also looks promising for detailed analyses of the development of secondary vortices in turbine cascades.

However, DNS is not yet a practical design tool, nor is highly-resolved LES, and design iterations are generally carried out by using more conventional RANS. The works of Denton and Pullan [15] and Pullan et al. [16] are example of successful applications of RANS/URANS analyses for the study of secondary flow features. They have shown how the impact of the unsteadiness to cascade end-wall loss is likely to be small.

In this work we concentrate on the test case documented in [17] that covers a range of Reynolds numbers and operating conditions and offers measurements both at mid-span and close to end-walls. In particular we focused on the $Re = 120k$ case with parallel end-walls mostly to reduce the LES computational effort. The measurements include pressure distributions around the airfoil at different span heights and span-wise distribution of losses. The simulations are carried out by both RANS, due to its continuing role as the design verification workhorse, and highly-resolved LES to

determine whether Reynolds Averaged models can capture the relevant flow details with a degree of accuracy able to drive the design of this crucial flow region. The decision was made to perform RANS and not URANS, as the latter are still quite computationally intensive and not routinely used in design iterations. Moreover, while URANS do predict vortex shedding, the resulting vortices decay at a much lower pace as compared with LES [18]. The comparison between the two approaches has been made fair and consistent by a careful evaluation of boundary conditions and grid density, and the use of start-of-the-art RANS modelling. In order to cope with the low Reynolds-number condition of the considered case, a state-of-the-art transition model [19] has been adopted in conjunction with a linear eddy viscosity closure for turbulence. The deviations of RANS results from the measurements by Duden and Fottner [17] are scrutinized with the help of the LES that provides a much deeper insight into the flow field as compared with test data. Part II of the paper focuses on the loss generation associated with the secondary end-wall vortices. In particular, entropy generation and the consequent stagnation pressure losses are analyzed following the aerodynamic investigation carried over in the companion paper [20]. This gives the opportunity to determine whether the common turbulence models generally used in RANS are able to discern the loss contributions of the different vortical structures identified by LES. The possible weaknesses of RANS in reproducing those features are also identified in order to focus the attention on aspects that needs further modelling efforts. This is a crucial issue for the improvement of RANS/URANS tools to be used for driving the design of modern LPTs for aeroengines, as the current turbine maturity level force designers to look for efficiency improvements that amount to few tenths of a point.

DESCRIPTION OF THE TEST CASE

The experimental study of the T106 cascade by Duden and Fottner [17] has been chosen as the best compromise between a realistic Reynolds $Re_{2,is} = 120k$ and Mach number ($M_{2,is} = 0.59$) on one hand, and affordability of several cases for a high resolution LES study on the other hand. The blade profile is the T106A with a pitch to chord ratio of 0.799 and an aspect ratio of 3. The inlet flow angle is 127.7 degree with respect to the pitch-wise direction. The downside of this study is that the inlet boundary layer state has only been reported in terms of boundary layer thickness, displacement thickness and momentum thickness. While some studies provide more detailed information like the mean flow profile and one RMS profile in wall normal direction, the authors are not aware of an end-wall flow study that fully determines the state in the boundary layer including anisotropy and length scales. The boundary layer profile used by Ciorciari et al. [21] who conducted a study in the same wind tunnel at a slightly lower Reynolds number is adopted for the present analysis (profile "C2" in part I [20]). In terms of integral quantities it is similar to the one of Duden and Fottner [17].

COMPUTATIONAL FRAMEWORK

The RANS Flow Solver. The TRAF code (Arnone [22]) was selected for the numerical RANS investigations. The code solves the unsteady, three-dimensional, Reynolds-averaged Navier-Stokes equations in the finite volume formulation on multi-block structured grids. Convective fluxes

are discretized by a 2nd order TVD-MUSCL strategy build on the Roe's upwind scheme. A central difference scheme is used for the viscous fluxes. The transition modelling is handled coupling the widely-used $\gamma - Re_{\theta,t}$ model proposed by Langtry and Menter [19] to the Wilcox $k-\omega$ turbulence model [23]. This model has been recently used to predict transitional flows in both high- and low-pressure turbine flows [12, 24].

The RANS Mesh. The computational domain was discretized using a O-H grid with $621\times101\times161$, and $81\times121\times161$ mesh points respectively, for a total of about 11.5 million cells. The mesh resolution in the blade-to-blade plane reflects the LES validation performed in [10, 25, 26], and the RANS validation summarized in [11, 12, 24]. The y^+ values of the mesh nodes closest to the wall are below 0.3 along the whole blade surface. The z^+ stands between 0.2 and 0.5 along the end-wall surface.

The LES Flow Solver. The LES were performed by using HiPSTAR, a multi-block fourth-order finite-difference solver based on a compact scheme and a fourth-order Runge-Kutta time marching algorithm. LES resolves the majority of small scale turbulent fluctuations thereby reducing the turbulence modeling effort typical of a RANS approach. The code was successfully validated for axial compressors, low pressure and high pressure turbines. Further details on the code can be found in Sandberg et al. [25] and in the companion paper [20].

The LES Mesh. The results presented in this part were obtained with the grid taken from Pichler et al. [26]. The span-wise resolution is set to have an end-wall wall-normal spacing of less than 1.5 in terms of plus unites in the entire domain and at least 150 points are in the boundary layers with a total of 855 points in the span-wise direction. Hence, the total number of points for the fine simulations are 497 Million that allowed a high-quality wall-resolved LES.

Boundary Conditions. The same boundary conditions were imposed for the RANS and the LES calculations. In particular at the computational domain inlet the swirl angle, the total pressure and the total temperature were assigned according to the inlet profile "C2" described in the companion paper [20]. LES and RANS inlet turbulence quantities are similar as in RANS the inlet turbulence length scale is fixed to mimic the LES inlet digital filter approach [20], and make sure turbulence in the two simulations decays at the same rate. Figure 1 shows the span-wise distributions of turbulent kinetic energy for the RANS calculation at two axial locations upstream the blade leading edge at $x/C_x = -0.25$ (Fig. 1(a)) and $x/C_x = -0.10$ (Fig. 1(b)). The comparison with the envelope of turbulent kinetic energy for various pitch-wise locations obtained in the LES simulation , shows

similar levels and similar decay rates far from the end-wall, while in the boundary layer the LES simulation presents values that are almost twice the ones found in the RANS case. A span-wise distribution of constant static pressure corresponding to $M_{2,is} = 0.59$ was imposed at the domain exit.

RESULTS AND DISCUSSION

The main purpose of this section is to identify differences in the RANS and LES predictions of secondary flows and determine whether these could jeopardize the accuracy and reliability of a RANS based design.

Vorticity Contour Plots

Prior to the discussion on the development of secondary flows, it is worthwhile to analyze Fig. 2, which illustrates an important specific feature of flow field. The cross section taken at $x/C_x = 1.03$ downstream of the trailing edge shows the stream-wise vorticity field. Such a quantity is calculated as:

$$\Omega_s = \Omega_x \cos\alpha_2 + \Omega_y \sin\alpha_2 \tag{1}$$

where α_2 is the average exit flow angle. The red surface (labelled "Sep") is a zero axial-velocity iso-surface associated to the dividing streamline of the separated shear layer of the suction side separation bubble discussed in the companion paper [20]. It is the consequence of the low Reynolds-number and the strong adverse pressure gradient experienced by the suction side boundary layer downstream of the throat section as widely discussed in several previous works (Stieger at al. [27], Howell et al. [28]). The reported streamlines belong to two groups: the first one refers to streamlines originating in the end-wall flow at the inlet, while the other group contains streamlines that originate above the inlet boundary layer and travel along the blade suction surface at a span-wise position where the separation bubble is first formed. The large red vortex, labelled “P”, is the passage vortex. The blue region labelled "HS" identifies the suction side branch of the horseshoe vortex. Moving away from the lower end-wall one extra vortical structure appears: the separation vortex “S”. This is generated by the interaction of the suction side separation and the end-wall flow: the low momentum fluid of the forming separated shear layer is convected in the upward direction by the secondary velocity components and rolls up into a vortex which is transported downstream. A complementary discussion of this phenomenon can be found in the companion paper [20], where it is evidenced by streamlines near the blade suction side forming a tornado-like vortex. Although not reported in this paper, RANS results at higher Reynolds numbers, which are not affected by suction side boundary-layer separation, do not show such a feature, and this reinforces the reported argumentation about its generation. With this in mind, it is possible to move to Fig. 3 that follows the evolution of the stream-wise vorticity generation. The first of the five cross sections orthogonal to the turbine axis is in the vane passage at $x/C_x = 0.9$ Fig. 3(a), while the last one extends further downstream at $x/C_x = 1.5$ Fig. 3(e). At $x/C_x = 0.9$ the pressure side flow is very clean, while the suction side shows strong stream-wise vorticity. Moving from mid-span towards the end-wall direction it

is possible to detect first the separation vortex "S". This vortex is clearly visible in RANS, while in LES it appears to be slightly weaker. At this axial position the suction side branch of the horseshoe vortex "HS" is already moving away from the wall while rolling together with the passage vortex "P". The pressure side branch of the horseshoe vortex is also detectable and it is indicated by the label "HP" in Fig. 3(b). The corner vortex "C" remains stably in the corner region. Remarkably, RANS and LES predict very similar flow fields, with the only exception of the relative intensity of the "P" and "HP" vortices. The section at $x/C_x = 1.03$, immediately downstream of the trailing edge, shows again a fair agreement between RANS and LES. Still, RANS shows how the vortex cores are moving more rapidly away from the end-wall, as witnessed by the position of the "S", "HP", and "P" vortices are in RANS relative to LES. Although the position of the vortex core is controlled by its distance from the end-wall, LES predicts larger vortices. Another noticeable difference is the strength and position of the corner vortex "C". LES predicts a stronger passage vortex "P" which sits closer to the end-wall as compared to RANS. Therefore, the corner vortex's strength and penetration in the pitch-wise direction in LES is reduced if compared with RANS. This subtle difference may have an impact on the development of cavity flows. The pitch-wise position of the "HS" vortex is similar, although deep in the wake LES predicts a stronger stream-wise vorticity, with a potential effect on the interaction with the downstream bladerow. The situation does not change for $x/C_x = 1.1$ where RANS and LES predictions are similar, and RANS predicts vortices slightly further away from the end-wall. Section $x/C_x = 1.3$ is particularly important because it is where the leading edge of the downstream bladerow may sit. At this axial position the agreement between RANS and LES is remarkably good, and we can observe only a minor difference in the relative position of the "P" and "HS" vorticity centers, that remains stable up to $x/C_x = 1.5$. Therefore, in a rotor-stator interaction analysis, the downstream blade row would experience a similar level of secondary distortions in the incoming flow, with possibly similar implications on the deterministic unsteadiness level. This is important not only for the aerodynamic aspects of the stage performance, but also for acoustic emission characteristics.

Total Pressure Loss Span-Wise Profiles

Figure 4 shows comparisons between LES and RANS predictions in terms of span-wise distributions of total pressure loss coefficient at four axial locations downstream the trailing edge, corresponding to $x/C_x = 1.03$ (Fig. 4(a)), $x/C_x = 1.10$ (Fig. 4(b)), $x/C_x = 1.30$ (Fig. 4(c)), and $x/C_x = 1.50$ (Fig. 4(d)) respectively. For both the calculations, tangentially mass-averaged (MA) and mixed-out (MO) distributions are reported. In the last axial location ($x/C_x = 1.50$, Fig. 4(d)) experimental measurements by Duden and Fottner [17] are also reported. Total pressure losses from LES are larger across the whole span. In the mid-span region the difference between mass-averaged and mixed-out distributions is smaller for LES than for RANS. It could be argued that LES wakes are more mature and decayed as opposed to RANS, this issue will be discussed in a later section. This difference fades out at $x/C_x = 1.30$ (Fig. 4(c)), and becomes practically zero at $x/C_x = 1.50$ (Fig. 4(d)). Looking at Fig. 4, it looks like RANS predicts very well profile losses away from the wall, as the agreement between calculated and measured values is remarkable. Moving closer to the wall, differences are

visible for $z/H < 0.15$ at $x/C_x = 1.1$. LES always predicts larger losses, while the local difference between mixed-out and mass-averaged span-wise distributions predicted by RANS is similar to the one by LES. This indicates similar level of spreading of the secondary flow structures at this axial location. Observe how the span-wise penetration of secondary flows, witnessed by the span-wise position of the loss peak, is stronger for RANS. This is in agreement with the previous discussion of the stream-wise vorticity field (Fig. 3). Moving downstream at $x/C_x = 1.3$, the mixed-out loss peak predicted by LES moves further away from the wall, but its absolute value remains the same. Conversely, the mixed-out peak value from RANS grows substantially (approximately from 0.09 to 0.11). This is suspected to be a consequence of the fact that the mixed-out loss distribution is obtained by averaging in the tangential direction only, and not in the span-wise direction. Therefore, the growth of the peak value can be attributed to the development and span-wise migration of the secondary flow while moving downstream. As for the previous section, the loss patterns from LES and RANS agree remarkably well. The furthermost section at $x/C_x = 1.5$ shows a very good agreement between measurements and LES. RANS results are also in good agreement with experiments for $z/H > 0.1$, but smaller losses are predicted near the end-wall. At this axial location, the difference between mixed-out and mass-averaged profiles is very small. Therefore, both RANS and LES predict span-wise distributions with a similar level of residual secondary flow strength, although the loss levels in the wall proximity differ by around 40%. This is a potential problem not only to determine blade-row efficiency, but also to predict the carry-over effect on the downstream blade row.

Wake Losses

The previous analysis suggests that while RANS can predict a very realistic secondary flow structure, the associated loss level appears to be under-estimated both in terms of MA and MO values. As already observed, the discrepancy in the loss levels at mid-span could be related to different wake spreading predictions between LES and RANS. In order to investigate on this issue, tangential total pressure loss coefficient distributions are compared in Fig. 5 for three of the axial locations considered so far ($x/C_x = 1.1$, $x/C_x = 1.3$, and $x/C_x = 1.5$). Wakes from LES appear more mature and diffused than their RANS counterparts in all the reported locations. Despite the higher center-line peak observed in the RANS results the wider width of the LES wakes results in higher loss coefficients when tangentially averaged and this supports the observation made on the span-wise loss profiles (Fig. 4). The maximum difference in wake width and center-line loss peak is recorded for $x/C_x = 1.1$. Such a difference in the near wake structure is not surprising if we consider that a major part of the breakdown of the coherent structures brought about by the wake shedding occurs in this region. Such phenomena which are responsible for a strong contribution to the wake mixing, are captured by LES, but obviously not reproduced in RANS calculations. The relevant difference in the near wake structures tends to be reduced in the downstream locations, in line with the discussed trend of mass-averaged and mixed-out losses, but the discrepancy in loss profiles persists even at $x/C_x = 1.5$. For realistic axial gaps between subsequent blade rows this difference in wake maturity at mid-span could result in inaccuracies in time-accurate simulations of rotor-stator interaction, especially if the residual wake mixes in a variable pressure environment (e.g. Praisner et al. [29]).

Turbulent Kinetic Energy Span-Wise Profiles

In order to gain further insights in the loss generation processes predicted by the two numerical analyses, it is convenient to look at comparisons among the turbulent kinetic energy and Reynolds stresses calculated by RANS and the ones resolved by LES.

Figure 6 compares the span-wise distributions of tangentially mass-averaged turbulent kinetic energy at the same axial locations considered for the loss profiles. Due to the very high grid resolution adopted in LES, the resolved TKE is more than 98% of the total TKE. At mid-span, LES predicts TKE levels above those given by RANS, although this difference quickly fades out and vanishes at $x/C_x = 1.5$. This trend agrees well with the mid-span level of losses observed before. It appears that the slightly larger mid-span losses predicted by LES is caused by a later decay of the higher TKE level visible at $x/C_x = 1.03$ (Fig. 6(a)). The picture changes moving close to the wall where LES indicates values that can be above or below RANS. The local production is clearly different, although the differences are limited, as expected when looking at the similar loss levels. Again, discrepancies tend to become minor for $x/C_x > 1.3$, but the stronger penetration of the secondary flows, that matches well with the loss profiles, is evident at $x/C_x = 1.5$.

Turbulent Stresses Span-Wise Profiles

Figure 7 compares the normal Reynolds Stress components from LES and RANS at $x/C_x = 1.1$ and $x/C_x = 1.3$. Here, for the sake of conciseness, only two axial locations are considered: $x/C_x = 1.1$ (Figs. 7(a), (b), and (c)) and $x/C_x = 1.3$ (Figs. 7(d), (e), and (f)). The levels of turbulence anisotropy (i.e. the difference between the normal stresses) are remarkably different. The τ_{11} component from RANS remains above the LES levels up to the $x/C_x = 1.3$ section at mid-span (Figs. 7(a), and (d)). Surprisingly, both the tangential and span-wise components are in much better agreement with LES away from walls (Figs. 7(b), (c), (e), and (f)). Moving close the wall, while the absolute levels at $x/C_x = 1.1$ are not identical, the profiles agree very well, and the differences fade out almost entirely at $x/C_x = 1.3$, an axial position near which the leading edge of the next blade row is expected to sit.

Figure 8 concentrates on the comparison among turbulent shear stresses in the same axial locations. The profiles reflect the secondary flow structure discussed above. τ_{13} and τ_{23} (the two shear stress components that contain the spanwise direction) show a general good agreement between LES and RANS. The vanishingly small values for $z/H > 0.2$ refer to the quasi-2D portion of the flow field that is not affected by the secondary flows and remains span-wise homogeneous. Some differences are visible for $z/H < 0.2$, although the agreement remains good. The τ_{12} component in the blade-to-blade plane behaves differently, as RANS shows an underprediction with respect to LES at $x/C_x = 1.1$ that reduces moving downstream to $x/C_x = 1.3$. As

τ_{12} is the main driver of the wake diffusion, such difference is responsible for the low wake decay typically predicted by RANS. A similar behavior was documented by Michelassi et al. [30], where the URANS-DNS Reynolds stress difference peaked close to the profile trailing edge and slowly reduced downstream. With reference to Fig. 4, we can conclude that the misprediction of losses in the proximity to the endwall ($z/H < 0.1$) is due to the differences in the turbulent shear stress components evidenced in Fig. 8.

Loss Generation

We can now proceed to the analysis of the 2D maps of losses in Fig. 9. At section $x/C_x = 0.9$ (Fig. 9(a)) RANS and LES predict again similar levels of total pressure loss, although it is possible to distinguish only the vortices with the largest associated losses (i.e. "P", "C", and "HP"). When moving downstream, RANS and LES can be seen to predict similar loss patterns, but with different magnitudes. Not surprisingly RANS predicts greater losses away from the end-wall. The difference in the overall loss pattern is small, but while the portion of the flow affected by a relevant loss level diffuses into the undisturbed flow in LES, RANS does predict stronger loss gradients and sharper lossy regions. This difference does not seem to fade away moving further downstream, as LES predicts higher loss levels in the $z/H < 0.15$ region from $x/C_x = 1.03$ on, and RANS never recover the same loss levels predicted by LES. Notably, the $x/C_x = 1.3$ section shows similar loss structures with higher losses from LES for $z/H < 0.15$. Now that the differences between and LES and RANS in terms of both span-wise plots (see Fig. 4) and 2D maps (see Figs. 3-9) have been illustrated, we can conclude that, on a single row basis, RANS replicates the LES results with a fair degree of accuracy. Nevertheless, the visible difference in the predictions of the flow field at $x/C_x = 1.3$ may have an impact on the design and performance prediction of the downstream blade-row. To further investigate this aspect, it is instructive to plot the span-wise distribution of the difference between the pitch-wise mixed-out losses (ω_{MO}) and the pitch-wise mass-averaged losses (ω_{MA}) at a specified axial location. When wakes and secondary flows have completely decayed there will be no additional losses. In this condition ω_{MO} equals ω_{MA}. So, a good measure of the "maturity" of the secondary flows, i.e. wakes and end-wall vorticity, is the difference $\omega_{MO} - \omega_{MA}$ reported in Fig. 10. LES and RANS are in good agreement for $z/H < 0.1$, but further away from the wall the already pointed out weakness of RANS, (i.e. the inability to predict the correct rate of wake diffusion) is visible. In fact, RANS predicts levels of $\omega_{MO} - \omega_{MA}$ larger than LES, that correspond to the less diffused and stronger wakes (see Fig. 5). This measure is important since, as discussed by Praisner et al. [29], Michelassi et al. [10], and Pichler et al. [31], the residual strength of incoming wakes at the leading edge of a turbine blade-row is directly proportional to the additional unsteady losses due to incoming wakes dilation. In case these additional unsteady losses are to be accounted for in a CFD assisted design, and RANS is likely to overpredict them as compared to LES. It is difficult to determine the magnitude of such overestimation, but looking at the LES from Pichler et al. [31] and the CFD from Praisner et al. [29], this could be worth 0.1% to 0.2%, a value that cannot be considered negligible with the current turbine design maturity level. Another subtle discrepancy occurs close to the end-wall where RANS predicts a higher peak with respect to LES. This may impact on the downstream end-wall boundary layer structure which is also important for the interaction with the downstream blade row.

In order to complete the investigation on the loss generation process reproduced in the two numerical analyses, dissipation coefficient contours by RANS and LES are compared in Fig. 11 for three key axial locations downstream the trailing edge ($x/C_x = 1.03$, $x/C_x = 1.1$, and $x/C_x = 1.3$). The dissipation coefficient computed with the mean flow field is defined as:

$$C_D = \frac{1}{\rho_{2,is} c_{2,is}^3} (\tau_{ij,\ell} + \tau_{ij}) \frac{\partial u_i}{\partial x_j} \tag{2}$$

and gives a measure of the local entropy production rate associated to the work by stresses. Immediately downstream the trailing edge ($x/C_x = 1.03$) the majority of the entropy generation still occurs in the PS and SS boundary layer regions, but LES shows a dissipation production region in the first 15% of the span which is barely detectable in RANS. This is consistent with the greater turbulence production by LES in this region (see Figs. 6(a) and (b)) and the associated differences in loss figures between LES and RANS (Figs. 4-9). At $x/C_x = 1.1$ the general picture is very similar to the previous one, with LES not surprisingly showing a higher mixing level of wakes and a pronounced loss production zone in the secondary flow region, with visible entropy generation cores corresponding to the passage and horseshoe vortices. The situation changes substantially at $x/C_x = 1.3$. Here the loss generation contributions by the secondary vortices can still be clearly distinguished, but while RANS sees the majority of entropy generation near the horseshoe vortex ("HS") core, LES associates the more intense dissipation production with the effects of the passage vortex "P". The contribution of the HS vortex in LES results appears to be confined in the first 15% of the span. Another difference concerns the corner vortex "C". In fact, while its contribution to entropy production is practically negligible in LES, a fairly high level of loss production associated with this flow features is visible in RANS results. Differences in the tangential extent and strength of the corner vortex in LES and RANS were already noticed when looking at stream-wise vorticity maps (Fig. 3) The dissipation coefficient maps are consistent with the loss distribution scenario discussed with the aid of span-wise profiles and 2D loss coefficient maps (Figs. 4-9). They also support the different span-wise distributions of loss potential obtained with the two numerical approaches (Fig. 10). In fact, the higher loss potential experienced in the RANS results between 10% and 20% span, is associated with secondary loss generation cores that in RANS are located at greater distances from the end-wall, while the higher peak close to the end-wall in RANS distribution is associated with the contribution of the corner vortex.

Figure 12 compares measurements [17] with both RANS and LES predictions of the axial evolution of mass-averaged total pressure loss coefficients inside the blade passage and downstream the trailing edge. Total and secondary loss coefficients are compared following the secondary loss definition adopted by Duden and Fottner [17]:

$$\omega_S = \omega - \omega_P - \omega_1 \tag{3}$$

where ω_P are the profile losses and ω_1 are the losses associated with the inlet boundary layer defect. The two distributions of total loss coefficient are extremely similar inside the blade passage, but they become different just after the trailing edge. Instead, secondary loss coefficient are practically coincident even far downstream the trailing edge. The direct comparison with Fig. 4(d) suggests that RANS total losses are smaller than LES and

measurements mostly due to the loss underestimation in the $z/H < 0.15$ region, while above the agreement between the simulations and measurements improves. This suggests that the different loss production mechanisms observed in the two numerical analyses play a minor role when integrated secondary losses are compared on a mass-averaged basis (i.e. the regions where important differences in loss distributions are located have a minor weight in the mass-averaging process). Moreover, although the definition of secondary losses of Eq.3 suggests a good agreement between LES, RANS, and measurements, the full loss profile of Fig. 4(d) proves that some not negligible differences still exist. The most relevant differences occur in the profile losses downstream the blade passage and arise in a short distance after the trailing edge. Actually, for $x/C_x > 1.1$ the rate of increase of total losses is practically the same in LES and RANS, but LES losses remain on a higher level. Such differences are not surprising in the light of the previous discussions, and they are probably related to the strong mixing predicted by LES in the trailing edge region. In fact, The majority of wake mixing is seen to occur rapidly downstream the trailing edge in LES calculations, while it is deferred, more gradual, and weaker in RANS. The better agreement of LES total integrated losses with downstream measurements relative to RANS can be regarded as another proof of RANS weakness in reproducing wake mixing process.

CONCLUDING REMARKS

The T106A blade in a linear cascade configuration with parallel end-walls has been analyzed with both RANS and LES to investigate the details of the secondary flow structure. In particular, part II of the paper is devoted to the analysis of loss generation by the end-wall secondary flow. The simulations are carried out by state-of-the-art RANS and LES approaches, both previously validated in similar flows. This gives the opportunity to determine whether the classical linear turbulence models generally used in RANS are able to discern the loss contributions of the different vortex structures identified by a well resolved LES. The purpose was to determine whether the possible discrepancies could jeopardize the accuracy and reliability of a RANS assisted design.

A detailed flow analysis based on the stream-wise vorticity field allows one to conclude that RANS and LES predict very similar secondary flow patterns, even if the span-wise penetration of secondary vortices is visibly stronger in the RANS results. Minor differences were found at axial locations where the downstream blade row leading edge usually sits. Therefore RANS and LES predict similar deterministic unsteadiness to the downstream blade row. In terms of loss distributions, predictions by RANS are again very realistic, but both the mass averaged and mixed-out loss level appears to be slightly underestimated. The direct comparison of turbulent kinetic energy, Reynolds stresses, and dissipation coefficient distributions revealed a good overall agreement between the two methods, although some key differences arose especially for the turbulent quantities. Such disagreements appear to have a relevant influence in the loss distribution in the proximity of the end-wall. This is a potential problem in the design of multi-blade row turbines where it is necessary to predict the carry-over effect on the downstream blade row. Conversely, such detailed differences seem to have a negligible influence on the development of bulk secondary losses, as they are found to be coincident for RANS and LES in the whole computational

domain.

The most important differences have been found to come from the wake development. RANS showed a weak and gradual wake maturation, while LES predicts a faster wake mixing and losses tend to a mixed-out value quicker. The different wake mixing mechanisms result in a higher loss level detected by LES for a single blade row. In case unsteady calculations are performed to verify multi-blade-row efficiencies, the different wake decay may cause an incorrect split of wake mixing losses at constant pressure (i.e. in the stator-rotor gap) versus wake mixing losses at variable pressure (i.e. in the vane of blade passage). Such differences will have an impact on both blade forced response and noise. Overall, this suggest that further modelling efforts should focus on the reproduction on wake structure and decay as this is the flow feature where RANS shows a major weakness.

ACKNOWLEDGMENTS

The authors gratefully acknowledge Baker Hughes, a GE Company for granting the permission to publish this paper. The compute time for the LES has been provided by the Pawsey Supercomputing center in Perth, Australia, and the Swiss national supercomputing center CSCS in Lugano, Switzerland. The work in the University of Melbourne was conducted under a GE research grant.

NOMENCLATURE

c velocity magnitude

C_D dissipation coefficient

C_x axial chord

H blade height

k turbulent kinetic energy

M Mach number

p pressure

$\tilde{Re}_{\theta,t}$ local transition onset momentum thickness Reynolds number

Re Reynolds number

s spacing

T temperature

u_i velocity field

x, y, z Cartesian coordinates

Greek

α flow angle

γ intermittency

θ boundary layer momentum thickness

ρ density

τ_{ij} Reynolds stress

Ω vorticity

ω loss coefficient, $\omega = (p_{01} - p_{02})/(p_{01} - p_2)$;

specific turbulence-dissipation rate

Ω_S stream-wise vorticity,

ω_S secondary loss coefficient, $\omega_S = \omega - \omega_P - \omega_1$

Subscripts and Superscripts

0 total quantity

1, 2 cascade up- and downstream conditions

ℓ laminar

is isentropic

P profile

S secondary

Acronyms

CFD Computational fluid dynamics

DNS Direct numerical simulation

LE Leading edge

LES Large eddy simulation

LPT Low pressure turbine

MA Mass-averaged

MO Mixed-out averaged

MUSCL Monotonic upwind scheme for conservation laws

PS Pressure side

RANS Reynolds-averaged Navier-Stokes

RMS Root-mean square

SS Suction side

TE Trailing edge

TKE Turbulent kinetic energy

TVD Total variation diminishing

REFERENCES

[1] Popović, I. and Hodson, H. P., 2013, "Aerothermal Impact of the Interaction Between Hub Leakage and Mainstream Flows in Highly-Loaded High Pressure Turbine Blades". ASME J. Turbomach., **135**(6), p.061014.

[2] Hodson, H. P. and Dominy, R. G., 1987, "Three-Dimensional Flow in a Low-Pressure Turbine Cascade at Its Design Condition". ASME J. Turbomach., **109**(2), pp. 177–185.

[3] Hodson, H. P. and Dominy, R. G., 1987, "The Off-Design Performance of a Low-Pressure Turbine Cascade". ASME J. Turbomach., **109**(2), pp. 201–209.

[4] Gregory-Smith, D. G., Graves, C. P., and Walsh, J. A., 1988, "Growth of Secondary Losses and Vorticity in an Axial Turbine Cascade". ASME J. Turbomach., **110**(1), pp. 1–8.

[5] Walsh, J. A. and Gregory-Smith, D. G., 1990, "Inlet Skew and the Growth of Secondary Losses and Vorticity in a Turbine Cascade". ASME J. Turbomach., **112**(4), pp. 633–642.

[6] Gregory-Smith, D. G. and Cleak, J. G. E., 1992, "Secondary Flow Measurements in a Turbine Cascade With High Inlet Turbulence". ASME J. Turbomach., **114**(1), pp. 173–183.

[7] Infantino, D., Satta, F., Simoni, D., Ubaldi, M., Zunino, P., and Bertini, F., 2015, "Phase-Locked Investigation of Secondary Flows Perturbed by Passing Wakes in a High-Lift LPT Turbine Cascade". ASME Turbo Expo. Montreal, Quebec, Canada, June 15–19, 2015. Paper No. GT2015-42480, pp. V02CT44A008.

[8] Sieverding, C. H., 1985, "Recent Progress in the Understanding of Basic Aspects of Secondary Flows in Turbine Blade Passages". ASME J. Eng. Gas Turbines Power, **107**(2), pp. 248–257.

[9] Langston, L. S., 2001, "Secondary Flows in Axial Turbines – A Review". Annals of the New York Academy of Sciences, **934**, pp. 11–26.

[10] Michelassi, V., Chen, L.-W., Pichler, R., Sandberg, R. D., and Bhaskaran, R., 2016, "High-Fidelity Simulations of Low-Pressure Turbines: Effect of Flow Coefficient and Reduced Frequency on Losses". ASME J. Turbomach., **138**(11), p.111006.

[11] Pacciani, R., Marconcini, M., Fadai-Ghotbi, A., Lardeau, S., and Leschziner, M. A., 2011, "Calculation of High-Lift Cascades in Low Pressure

Turbine Conditions Using a Three-Equation Model". ASME J. Turbomach., **133**(3), p.031016.

[12] Pacciani, R., Marconcini, M., Arnone, A., and Bertini, F., 2014, "Predicting High-Lift LP Turbine Cascades Flows Using Transition-Sensitive Turbulence Closures". ASME J. Turbomach., **136**(5), p.051007.

[13] Koschichow, D., Froehlich, J., Kirik, I., and Niehuis, R., 2014, "DNS of the Flow Near the Endwall in a Linear Low Pressure Turbine Cascade With Periodically Passing Wakes". ASME Turbo Expo. Düsseldorf, Germany, June 16–20, 2014. Paper No. GT2014-25071, pp. V02DT44A001.

[14] Cui, J., Nagabhushana, R., and Tucker, P. G., 2017, "Numerical Investigation of Secondary Flows in a High-Lift Low Pressure Turbine". Int. J. Heat Fluid Flow, **63**, pp. 149–157.

[15] Denton, J. and Pullan, G. P., 2012, "A Numerical Investigation Into the Sources of Endwall Loss in Axial Flow Turbines". ASME Turbo Expo. Copenhagen, Denmark, June 11–15, 2012. Paper No. GT2012-69173, pp. 1417-1430.

[16] Pullan, G. P., Denton, J. D., and Dunkley, M., 2003, "An Experimental and Computational Study of the Formation of a Streamwise Shed Vortex in a Turbine Stage". ASME J. Turbomach., **125**(2), pp. 291–297.

[17] Duden, A. and Fottner, L., 1997, "Influence of Taper, Reynolds Number and Mach Number on the Secondary Flow Field of a Highly Loaded Turbine Cascade". P. I. Mech. Eng. A-J. Pow., **211**(4), pp. 309–320.

[18] Sandberg, R., Tan, R., Weatheritt, J., Ooi, R., Haghiri, A., Michelassi, V., and Laskowski, G., 2018, "Applying Machine Learnt Explicit Algebraic Stress and Scalar Flux Models to a Fundamental Trailing Edge Slot". ASME Turbo Expo. Oslo, Norway, June 11–15, 2018. Paper No. GT2018-75444, pp. V05AT12A007.

[19] Langtry, R. B. and Menter, F. R., 2009, "Correlation-Based Transition Modeling for Unstructured Parallelized Computational Fluid Dynamics Codes". AIAA J., **47**(12), pp. 2894–2906.

[20] Pichler, R., Zhao, Y., Sandberg, R. D., Michelassi, V., Pacciani, R., Marconcini, M., and Arnone, A., 2018, "LES and RANS Analysis of the End-Wall Flow in a Linear LPT Cascade: Part I – Flow and Secondary Vorticity Fields Under Varying Inlet Condition". ASME Turbo Expo. Oslo, Norway, June 11–15, 2018. Paper No. GT2018-76233, pp. V02BT41A020.

[21] Ciorciari, R., Kirik, I., and Niehuis, R., 2014, "Effects of Unsteady Wakes on the Secondary Flows in the Linear T106 Turbine Cascade". ASME J. Turbomach., **136**(9), p.091010.

[22] Arnone, A., 1994, "Viscous Analysis of Three–Dimensional Rotor Flow Using a Multigrid Method". ASME J. Turbomach., **116**(3), pp. 435–445.

[23] Wilcox, D. C., 1998, *Turbulence Modeling for CFD*, 2nd edition, DCW Ind. Inc., La Cañada, CA, USA, ISBN 1-928729-10-X.

[24] Marconcini, M., Pacciani, R., and Arnone, A., 2015, "Transition Modelling Implications in the CFD Analysis of a Turbine Nozzle Vane Cascade Tested Over a Range of Mach and Reynolds Numbers". J. Therm. Sci., **24**(6), pp. 526–534.

[25] Sandberg, R. D., Michelassi, V., Pichler, R., Chen, L.-W., and Hohnston, R., 2015, "Compressible Direct Numerical Simulation of Low-Pressure Turbines - Part I: Methodology". ASME J. Turbomach., **137**(5), p.051011.

[26] Pichler, R., Sandberg, R. D., and Michelassi, V., 2016, "Assessment of Grid Resolution Requirements for Accurate Simulation of Disparate Scales of Turbulent Flow in Low-Pressure Turbines". ASME Turbo Expo. Seoul, South Korea, June 13–17, 2016. Paper No. GT2016-56858, pp. V02CT39A030.

[27] Stieger, R. D. and Hodson, H. P., 2004, "The Transition Mechanism of Highly Loaded Low-Pressure Turbine Blades". ASME J. Turbomach., **126**(4), pp. 536–543.

[28] Howell, R. J., Ramesh, O. N., Hodson, H. P., Harvey, N. W., and Schulte, V., 2001, "High Lift and Aft–Loaded Profiles for Low–Pressure Turbines". ASME J. Turbomach., **123** (2), pp. 181–188.

[29] Praisner, T. J., Clark, J. P., Nash, T. C., Rice, M. J., and Grover, E. A., 2006, "Performance Impacts Due to Wake Mixing in Axial-Flow Turbomachinery". ASME Turbo Expo. Barcelona, Spain, May 8–11, 2006. Paper No. GT2006-90666, pp. 1821-1830.

[30] Michelassi, V., Chen, L.-W., Pichler, R., and Sandberg, R. D., 2015, "Compressible Direct Numerical Simulation of Low-Pressure Turbines: Part II - Effect of Inflow Disturbances". ASME J. Turbomach., **137**(7), p.071005.

[31] Pichler, R., Michelassi, V., Sandberg, R. D., and Ong, J., 2017, "Highly Resolved LES Study of Gap Size Effect on Low-Pressure Turbine Stage". ASME J. Turbomach., **140**(2), p.021003.

LIST OF FIGURES

Figure 11: Dissipation coefficient contours in various axial locations (left RANS, right LES): (a) $x/C_x = 1.03$, (b) $x/C_x = 1.1$, (c) $x/C_x = 1.3$. (turbo-18-1214-fig11)

Figure 12: Mass-averaged total and net secondary loss coefficient evolution. (turbo-18-1214-fig12)

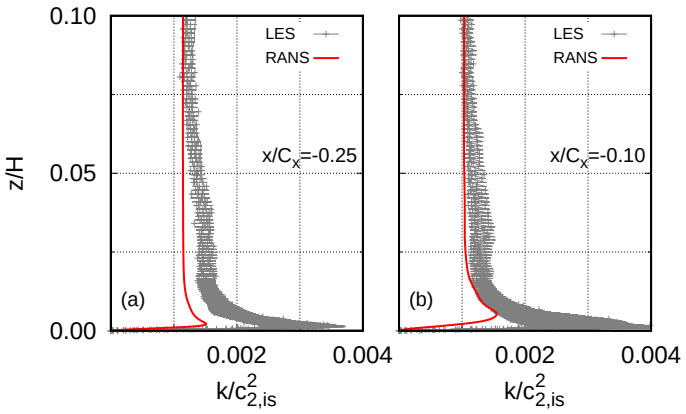

Figure 1: Span-wise distributions of turbulent kinetic energy at two axial locations upstream the leading edge.

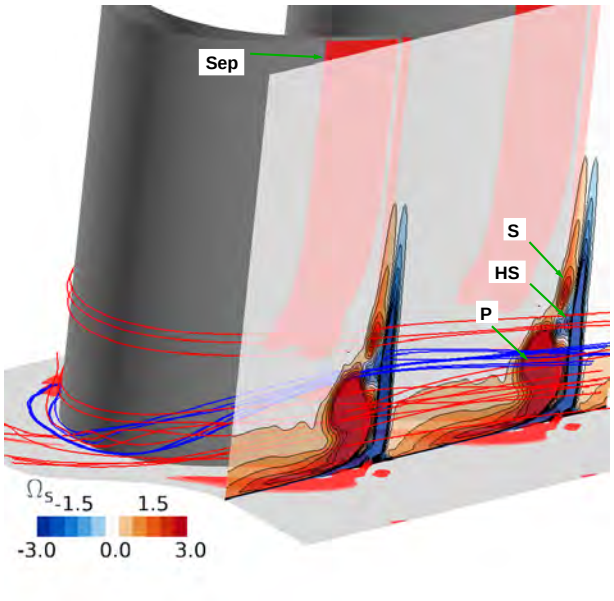

Figure 2: Stream-wise vorticity contours at $x/C_x = 1.3$ and iso-surface of zero axial velocity.

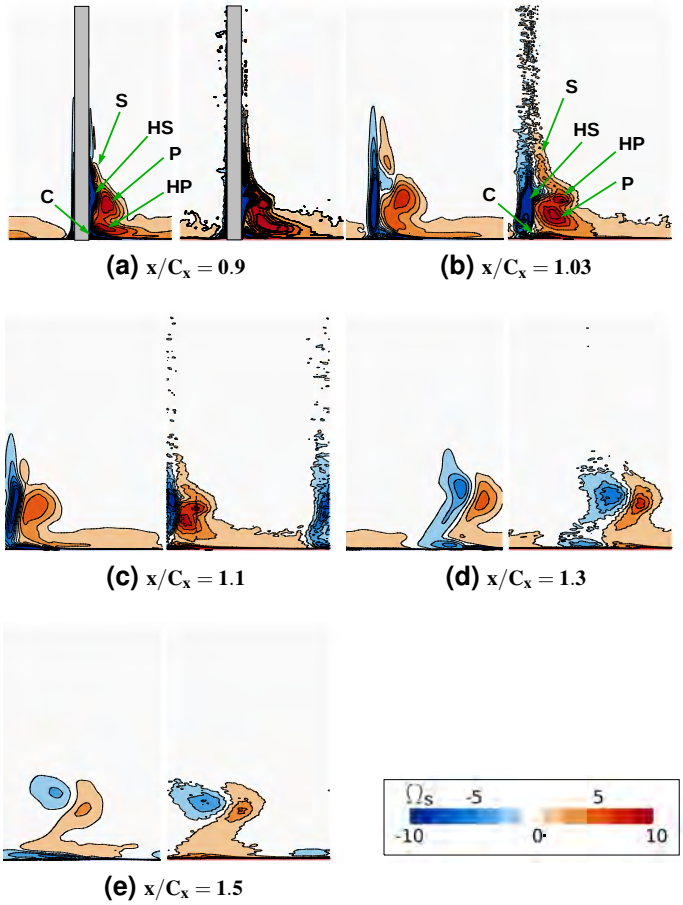

Figure 3: Stream-wise vorticity contours in various axial locations (left RANS, right LES): (a) $x/C_x = 0.9$, (b) $x/C_x = 1.03$, (c) $x/C_x = 1.1$, (d) $x/C_x = 1.3$, (e) $x/C_x = 1.5$.

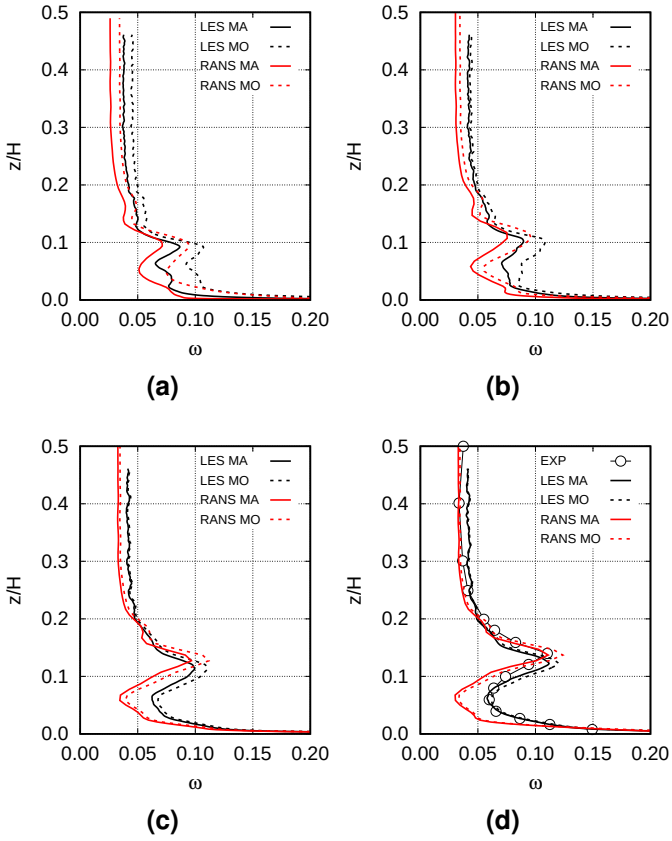

Figure 4: Span-wise distributions of total pressure loss coefficient at four axial locations (a) $x/C_x = 1.03$ (b) $x/C_x = 1.10$, (c) $x/C_x = 1.30$, (d) $x/C_x = 1.50$

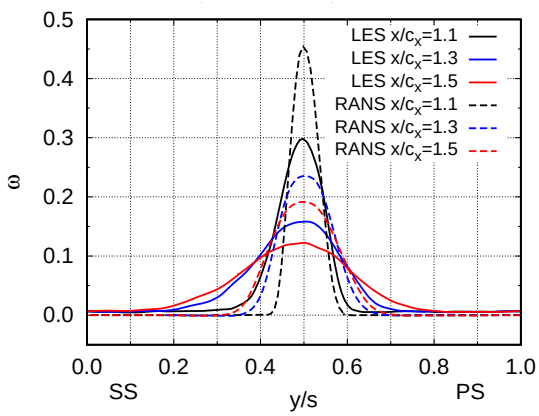

Figure 5: Tangential distributions of total pressure loss coefficient downstream the blade TE

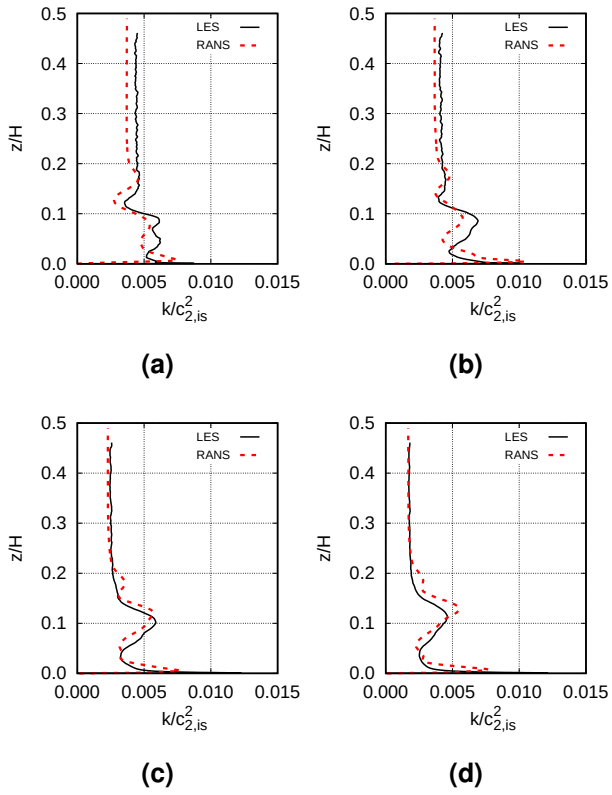

Figure 6: Span-wise distributions of turbulent kinetic energy at four axial locations: (a) $x/C_x = 1.03$, (b) $x/C_x = 1.1$, (c) $x/C_x = 1.3$, (d) $x/C_x = 1.5$,

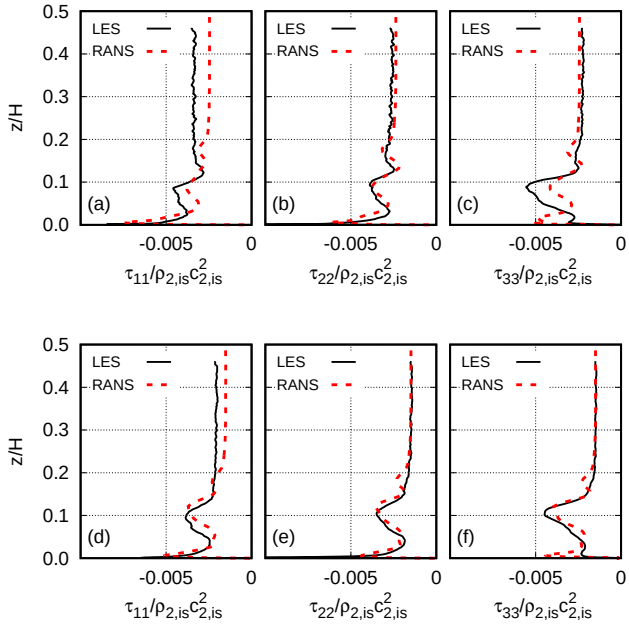

Figure 7: Span-wise distributions of normal Reynolds stresses at: $x/C_x = 1.1$ [(a), (b), (c)], and $x/C_x = 1.3$, [(d), (e), and (f)]

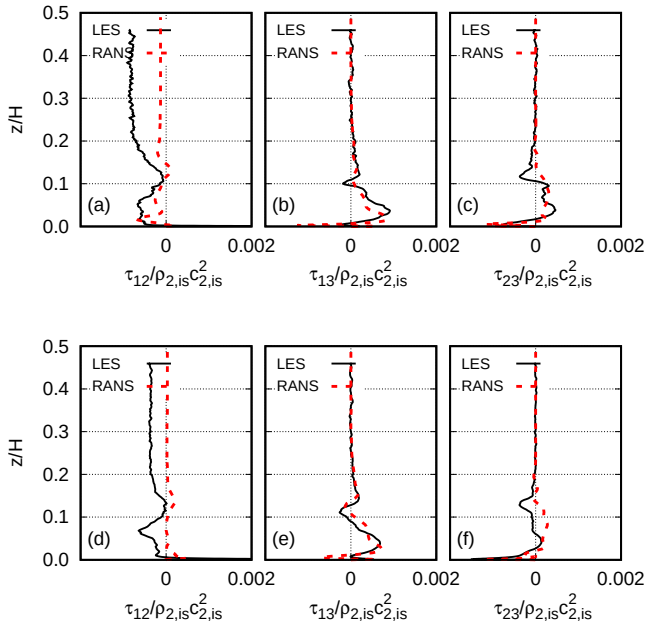

Figure 8: Span-wise distributions of shear Reynolds stresses at: $x/C_x = 1.1$ [(a), (b), (c)], and $x/C_x = 1.3$, [(d), (e), and (f)]

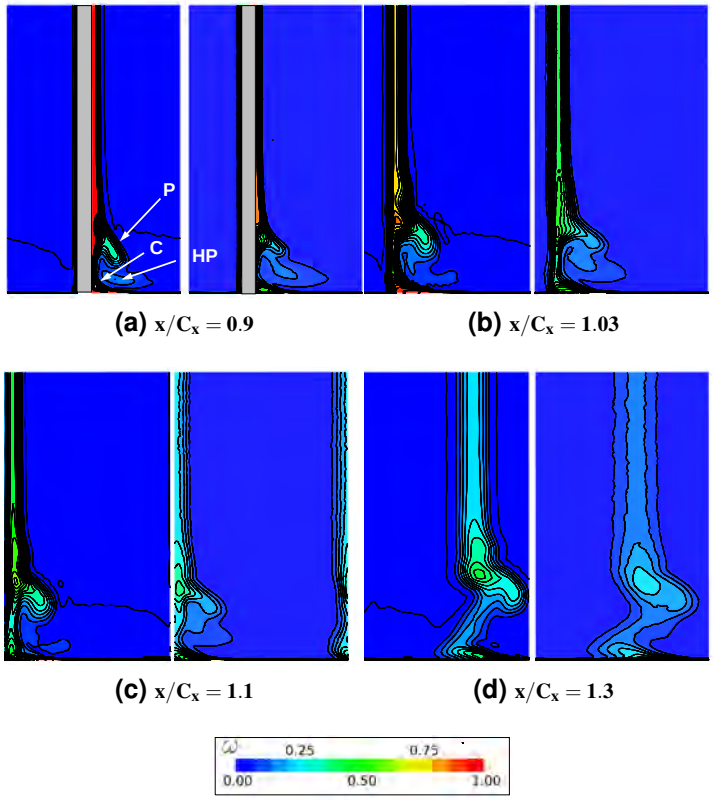

Figure 9: Loss coefficient contours in various axial locations (left RANS, right LES): (a) $x/C_x = 0.9$, (b) $x/C_x = 1.03$, (c) $x/C_x = 1.1$, (d) $x/C_x = 1.3$.

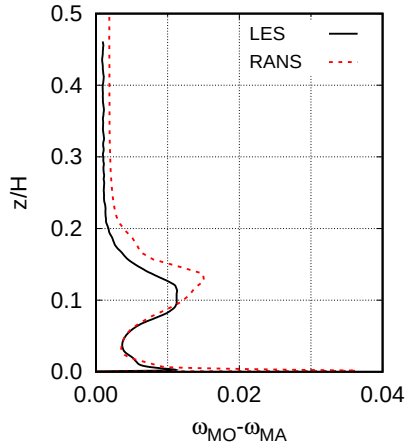

Figure 10: Span-wise distribution of loss potential at $x/C_x = 1.3$.

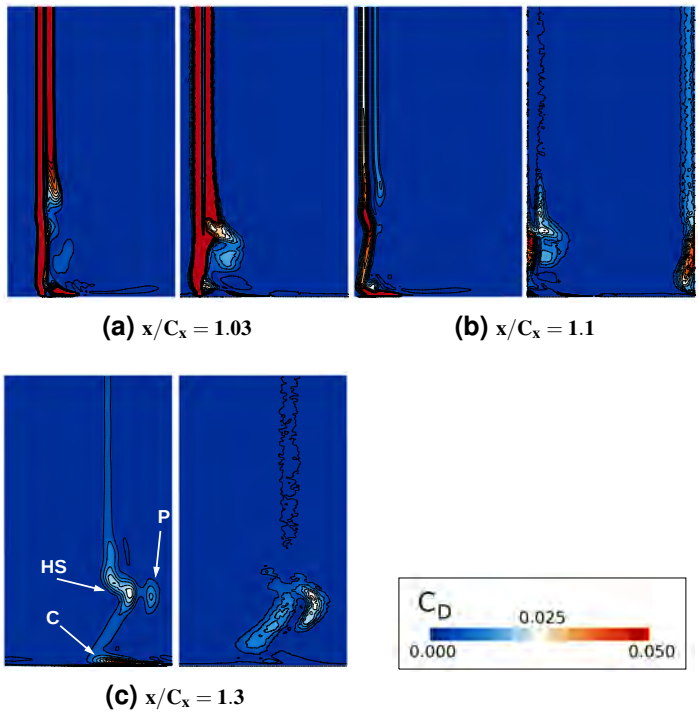

Figure 11: Dissipation coefficient contours in various axial locations (left RANS, right LES): (a) $x/C_x = 1.03$, (b) $x/C_x = 1.1$, (c) $x/C_x = 1.3$.

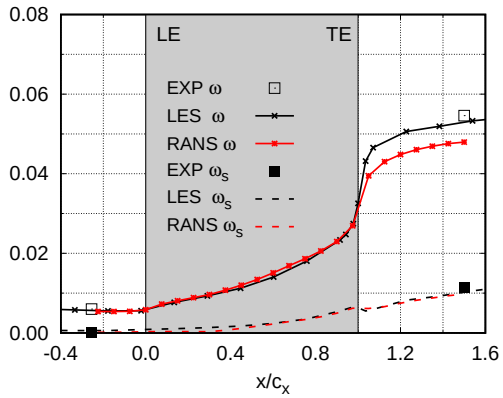

Figure 12: Mass-averaged total and net secondary loss coefficient evolution.

Author/s:
Marconcini, M;Pacciani, R;Arnone, A;Michelassi, V;Pichler, R;Zhao, Y;Sandberg, R

Title:
Large Eddy Simulation and RANS Analysis of the End-Wall Flow in a Linear Low-Pressure-Turbine Cascade-Part II: Loss Generation

Date:
2019-05-01

Citation:
Marconcini, M., Pacciani, R., Arnone, A., Michelassi, V., Pichler, R., Zhao, Y. & Sandberg, R. (2019). Large Eddy Simulation and RANS Analysis of the End-Wall Flow in a Linear Low-Pressure-Turbine Cascade-Part II: Loss Generation. Journal of Turbomachinery, 141 (5), https://doi.org/10.1115/1.4042208.